DESIGN OF OPTIMAL SPACECRAFT-ASTEROID FORMATIONS THROUGH A HYBRID GLOBAL OPTIMIZATION APPROACH

CHRISTIE ALISA MADDOCK

Space Advanced Research Team, Department of Aerospace Engineering
University of Glasgow, James Watt Building South,
Glasgow, United Kingdom, G12 8QQ
c.maddock@aero.gla.ac.uk
http://www.aero.gla.ac.uk/Research/SpaceArt

MASSIMILIANO VASILE

Space Advanced Research Team, Department of Aerospace Engineering
University of Glasgow, James Watt Building South,
Glasgow, United Kingdom, G12 8QQ
m.vasile@aero.gla.ac.uk
http://www.aero.gla.ac.uk/Research/SpaceArt

Received (Day Month Year)
Revised (Day Month Year)
Accepted (Day Month Year)

Abstract
The following paper presents the design of an optimal set of spacecraft formation orbits around an asteroid. The spacecraft are designed to fly in close proximity with the asteroid, avoiding its nonlinear gravity field. A behavioral-based hybrid global optimization approach is used to first characterize the solution space and find families of orbits that are a fixed distance away from the asteroid. The same optimization approach is then used to find the set of Pareto optimal solutions that minimize both the distance from the asteroid and the variation of the Sun-spacecraft-asteroid angle. The Near Earth Asteroid 99942 Apophis (2004 MN_4) is used as the case study due to a fly-by of Earth in 2029 leading to two potential impacts in 2036 or 2037.

Purpose – To present a methodology and experimental results on using global optimization algorithms to determine the optimal orbit, based on the mission requirements, for a set of spacecraft flying in formation with an asteroid.
Design/Methodology/Approach – Two sample missions to asteroids, representing constrained single and multi-objective problems, were selected to test the applicability of using an in-house hybrid stochastic-deterministic global optimization algorithm (EPIC) to find optimal orbits for a spacecraft flying in formation with an orbit. Two black-box optimization problems that model the orbital dynamics of the spacecraft were developed.
Findings – It was found for the two missions under test, that the optimized orbits fall into various distinct *families*, which can be used to design multi-spacecraft missions with similar orbital characteristics.
Research limitations/implications – The global optimization software, EPIC, was very effective at finding sets of orbits which met the required mission objectives and constraints for a formation of spacecraft in proximity of an asteroid. The hybridization of the stochastic search with the deterministic domain decomposition greatly improve the intrinsic stochastic nature of the multi-agent search process without the excessive computational cost of a full grid search. The stability of the discovered families of formation orbit is subject to the gravity perturbation of the asteroid and to the solar pressure. Their control, therefore, require further investigation.
Originality/value – This paper contributes to both the field of space mission design for close-proximity orbits and to the field of global optimization. In particular suggests a common formulation for single and multi-objective problems and a robust and effective hybrid search method based on behaviorism. This approach provides an effective way to identify families of optimal formation orbits.

Keywords Formation Flying, Constrained Global Optimization, Constrained Multiobjective Optimization, Asteroid Tracking and Deflection

Paper type Research paper

1. Introduction

The existence of asteroids and comets are nothing new to science. As the planets formed and their orbits began to stabilize, the collision rate among the drifting asteroids decreased dramatically, however has in no way stopped. As the population and occupied surface of the Earth increases, the impact of even a relatively small asteroid could be devastating. An asteroid spanning 200 m in diameter, for example, can produce a crater 4 km in size, assuming it only hits land and not water. The larger classes of asteroids, those over 1 km in diameter, are considered to be a global threat (ESA NEO Mission Advisory Panel, 2004).

It is of prime importance, therefore, to be able to identify and track, with a high degree of accuracy, the numerous Near Earth Objects (NEO) that exist in our solar system (Council of Europe, 1996; Global Science Forum, 2003). In tracking an object, it is important for the spacecraft to have an orbit that is in relative proximity to the asteroid at all times. On-board measuring systems, such as laser and radar tracking instruments determine the distance between the spacecraft and a particular spot on the surface of the asteroid. In the case of multiple spacecraft, and/or multiple readings by the same spacecraft over time, triangulation techniques can be easily applied to determine the ephemeredes of the asteroid with a high degree of accuracy.

Once our knowledge of the orbit of the asteroid is good enough to predict a possible impact, a deflection mission should be implemented. One possible option, first proposed by Melosh (1994), is to sublimate part of the surface of an asteroid by focusing sunlight with a space-based mirror. The sublimated material would be ejected thereby producing a thrust (the physical principle is similar to that of a rocket engine). The original idea hypothesized using a mirror more than one kilometer in diameter; such a huge structure however would be extremely difficult to launch and control. Another possible solution, proposed more recently by Maddock *et al.* (2007), is to use a swarm of spacecraft flying in formation with the asteroid. Each satellite can carry a relatively small mirror, only a few tens of meters, and focus a portion of the sunlight required to sublimate the surface of the asteroid. The accumulated effect would be the same as with one large mirror.

This paper presents the design and optimization of a set of orbits to allow a spacecraft to fly in formation with an asteroid orbiting around the Sun. The asteroid *99942 Apophis* was chosen as the test case based on its popularity in current media due to its probability of collision with the Earth. Compared to other near Earth objects, Apophis has a *relatively* high probability of impacting the Earth in April 2036, although the *actual* cumulative impact probability is low, only 2.2 E-5 (NASA NEO Program, 2008). Whether the asteroid will impact the Earth is contingent upon the asteroid's fly-by of Earth in 2029. Depending on the location and velocity of the asteroid relative to Earth, the orbit can be altered in many different ways. In the worst case, a few of the scenarios lead to an impact seven to eight years later.

As with nearly all NEOs, the orbital data for Apophis has been gained from Earth-based observations. These observations are limited due to the visibility of the asteroid

from the astronomy station, availability of the station, etc. (Chesley, 2005). As a result, the present knowledge of the orbit of Apophis is not sufficient to provide an accurate long term prediction of its evolution. This underlines the need for longer term measurements from a space-based platform (Schweickart, 2005).

Ideally the spacecraft should fly in formation with the asteroid at an almost constant distance from it. Finding the optimal set of initial conditions that provide a periodic motion with constant distance can be formulated as a constrained global optimization problem. A black box containing a model of the problem under investigation was programmed for the orbit of a single spacecraft flying in formation with the NEO. Two real-world applications were tested: the first mission tracks the asteroid, whereas the second, more complex mission, attempts to deviate the asteroid based on thrust generated by sublimating the surface of the asteroid.

In both cases it is desirable to have a collection of several optimal solutions, all with similar values of the objective function. Furthermore, the deflection problem requires both a constant distance and a constant solar aspect angle (i.e. Sun-spacecraft-Asteroid angle), thus, it can be formulated as a multiobjective problem. Normally in literature, single objective optimization and multiobjective optimization are treated as two distinct problems with different algorithms developed to address either one or the other.

Many approaches for both single and multiobjective optimization are biologically inspired. Some derive their inspiration from evolutionary processes, e.g. Coello *et al.* (2007), Price *et al.* (2005), Deb *et al.* (2000; 2002), while others from social behaviors in animals, e.g. Kennedy and Eberhart (1995), Elbeltagi *et al.* (2005), Reyes and Coello (2007). In this paper we used a unified formulation that can be applied to the solution of both single and multiobjective problems in which the aim is to find a set of optimal solutions rather than a single one. A hybrid deterministic-stochastic approach based on behaviorism was used to characterize the search space and to find the desired set of optimal solutions for both the tracking problem and for the deviation problem.

The stochastic part of the algorithm is based on a meta-heuristic that selects and implements an appropriate set of actions (i.e. heuristics derived from various bio-inspired approaches) for a small group of agents aimed at finding the optimal set. The deterministic part partitions the search domain, depending on the outcome of the stochastic part, and directs the search toward areas of the solution space that are either unexplored or particularly promising.

The following paper is broken down into four sections. The first details the design of the various models used in the simulation: the model of the asteroid, the orbital mechanics for the spacecraft, and the model for the deflection strategy. The second describes the formulation of the two design problems, and the third section details the behavior and characteristics of the hybrid global optimization method used. The final section lists the results of the simulations, and analyses the effectiveness at designing optimal asteroid-formation orbits.

2. Simulation Models

The following section describes the dynamical models used in simulating the orbit of a formation of spacecraft about a NEO, in this case the asteroid 99942 Apophis.

2.1. *Asteroid Model*

The current data on the characteristics of Apophis, originally designated 2004 MN_4, is based on a total of two radar delay measurements, five Doppler measurements and 731 optical observations over a period of 2.4 years. Data collection started in 2004, when the asteroid was first sighted. Table 1 and Fig. 1 give the orbital and physical data including an estimate of the margin of error on the observations (NASA NEO Program, 2007).

Table 1. Estimated and observed orbital and physical properties of Apophis 99942.

Fig. 1. Orbit of the NEO Apophis, compared to the orbits of the Mars, Earth and Venus. The top figure (a) illustrates the view of the ecliptic plane, while the bottom figure (b) shows the inclination difference between the orbits.

In a related study on a NEO deviation strategy (Maddock *et al.*, 2007), an analysis of the dynamical environment of Apophis was conducted in order to determine the feasibility of having the spacecraft orbit the asteroid by using the gravitational field of the asteroid (i.e. using the asteroid as the central body of the orbit). The model also compared the effects of third-body perturbations from the Sun and Apophis on the spacecraft in this scenario.

It was found that the perturbations near Apophis are either highly chaotic, or too weak relative to the solar effects to allow a spacecraft to easily orbit the asteroid. An alternative approach is to fly the spacecraft in close formation with Apophis; the spacecraft orbits around the Sun with the asteroid, but is not adversely affected by its presence.

2.2. *Equations of Motion*

For the orbit of the spacecraft, an initial solar orbit was set equal to that of the asteroid under study, Apophis. A spatial offset was introduced relative to the position of the asteroid at an arbitrary initial time, t_0. This offset acts like a periodic disturbance, in which the period of the oscillation is equal to that of the orbital period around the Sun. The end result is a relatively small formation orbit, which in turns orbits around the Sun (see Fig. 2). From a kinematics' point of view, the concept is similar to the orbit of the Moon; the Moon orbits about a central point, the Earth, which in turn both orbit as a system around the Sun.

Fig. 2. Illustration of a chief orbit and a relative deputy spacecraft orbit flying in formation at two instants in time, t and $(t+\Delta t)$. The vector from the Sun to the asteroid (or chief) in inertial coordinates is given by $\mathbf{r}_c$, and from the Sun to the formation, or deputy, spacecraft by $\mathbf{r}_d$.

Assuming the only forces acting on the spacecraft are caused by the gravity of the Sun, the relative equations of motion for the spacecraft are given by (Schaub and Junkins, 2003),

$$\begin{aligned}
\ddot{x}(t) &= 2\dot{\theta}\left(\dot{y} - y\frac{\dot{r}_c}{r_c}\right) + x\dot{\theta}^2 + \frac{\mu}{r_c^{\,2}} - \frac{\mu}{r_d^{\,3}}\left(r_c + x\right) \\
\ddot{y}(t) &= -2\dot{\theta}\left(\dot{x} - x\frac{\dot{r}_c}{r_c}\right) + y\dot{\theta}^2 + \frac{\mu}{r_c^{\,2}} - \frac{\mu}{r_d^{\,3}}y \\
\ddot{z}(t) &= \frac{\mu}{r_d^{\,3}}z
\end{aligned} \tag{1}$$

given

$$\mathbf{r}_d = \sqrt{\left(x + r_c\right)^2 + y^2 + z^2}\,\hat{\mathbf{r}}_d = \mathbf{r}_c + \mathbf{r}_{cd}$$

where $\mathbf{r}_c$ and $\mathbf{r}_d$ are the vectors from the Sun to the formation spacecraft ($_d$) and asteroid ($_c$) respectively, μ is the gravitational constant of the Sun, $\dot{\theta}$ is the angular rate of change of the solar orbit, and $\{x \quad y \quad z\}$ denote the relative rotating coordinate system, called a *Hill reference frame*, measured in the radial $\hat{x}$, transversal $\hat{y}$ and normal $\hat{z}$ directions. The origin of the relative reference system is positioned at the geometric center of the asteroid.

As can be clearly seen, these equations are inherently nonlinear, making it complex to find a closed form set of analytical solutions for the motion of the spacecraft.

An alternate form of representing the orbital motion are Keplerian elements, $\text{œ} = \begin{bmatrix} a & e & i & \Omega & \omega & \theta \end{bmatrix}^T$ where a is the semi-major axis, or a maximum distance from the geometric center of the orbit to a point along the orbital path, e is the eccentricity which is a measure of the circularity of the orbit ($e = 0$ being a perfect circle, and $e > 1$ being a hyperbola), i is the inclination of the orbital plane, and Ω and ω are angles determining the location of the line of intersection between the orbital plane and the reference plane, and orbital plane and periapsis respectively, and lastly θ is the true anomaly. The latter term is the only time-varying parameter, and represents the angle between the periapsis of the orbit (the location of the minimum distance from the focal point to the orbit path) and the actual location of the spacecraft at that point in time relative to the focal point of the orbit.

The general equations of motion given in Equation (1) can be linearly mapped from Cartesian Hill coordinates to a set of orbital elements by means of a transformation matrix A (Schaub and Junkins, 2003).

$$\chi = \left[A(\text{œ})\right] \cdot \delta\text{œ} \quad \Leftrightarrow \quad \delta\text{œ} = \left[A^{-1}(\text{œ})\right] \cdot \chi \tag{2}$$

where $\chi = \begin{bmatrix} x & y & z & \dot{x} & \dot{y} & \dot{z} \end{bmatrix}^T$ is the state vector containing the position and velocity components of the spacecraft in the Hill reference frame at a given time, and œ is the equivalent set of Keplerian elements. The difference between the solar orbit and

formation orbit is given by, $\delta\text{œ} = \text{œ} - \text{œ}_d$. For simplicity, the subscript '*c*' is dropped when working with the orbital element sets.

Using the equations above, a set of linearized equations for the relative orbital motion can be developed in order to propagate the state vector of the spacecraft forward in time. The equations of motion can be rearranged to use the true anomaly as the variable parameter instead of time. Indeed, using the rate of change of a central angle is preferable when working with periodic orbits, rather than simply propagating forward for a set amount of time (typically equal to the period of the orbit).

Moreover, Kepler's second law states that for a closed orbit "a satellite will sweep out equal areas in equal time" (Vallado, 2007). For an elliptical orbit, the true anomaly is not linearly varying with time as the velocity of the spacecraft is constantly changing depending on the position relative to the central body. Kepler's equation introduces an alternate angular measurement of the position of the spacecraft, the mean anomaly M , based on the mean angular velocity, n .

$$M = \int_{t_0}^{t_i} n \, dt = \sqrt{\frac{\mu}{a^3}} \left(t_i - t_0 \right) \tag{3}$$

where $\left(t_i - t_0 \right)$ is the time duration of the flight.

The mean anomaly corresponds to a uniform angular motion on an equivalent circle of radius equal to the semi-major axis, a , of the elliptical orbit. By replacing the difference in true anomaly with the difference in mean anomaly, δM , the equations can be written in a form which is more convenient when looking for periodic solutions.

A set of equations for the linearized relative motion represented by matrix A can then be developed based on the true anomaly of the solar orbit at time t (Schaub and Junkins, 2003),

$$
\begin{aligned}
x(\theta) &= \frac{r_c}{a}\cdot\delta a - a\cos\theta\cdot\delta e + \frac{ae\sin\theta}{\eta}\cdot\delta M \\
y(\theta) &= \frac{r_c\sin\theta}{\eta^2}\left(2+e\cos\theta\right)\cdot\delta e + r_c\cos i\cdot\delta\Omega + r_c\cdot\delta\omega + \frac{r_c}{\eta^3}\left(1+e\cos\theta\right)^2\cdot\delta M \\
z(\theta) &= r_c\sin(\theta+\omega)\cdot\delta i - r_c\cos(\theta+\omega)\sin i\cdot\delta\Omega \\
\dot{x}(\theta) &= \frac{-v_r}{2a}\cdot\delta a + \sqrt{\frac{\mu}{p}}\frac{e\cos\theta\left(1+e\cos\theta\right)^2}{\eta^3}\cdot\delta M \\
&\quad + \left(\frac{\sqrt{\mu p}\cos\theta\sin\theta\left(2+e\cos\theta\right)}{\eta^2} + v_r ae\sin(2\omega) + \sqrt{\frac{\mu}{p}}\sin\theta\right)\cdot\delta e \\
\dot{y}(\theta) &= \frac{-3v_t}{2a}\cdot\delta a + v_r\cos i\cdot\delta\Omega + \left(e\sin\theta\sqrt{\frac{\mu}{p}} - v_r\right)\cdot\delta\omega - \frac{v_r\left(1+e\cos\theta\right)^2}{\eta^3}\cdot\delta M \\
&\quad + \frac{2+e\cos\theta}{\eta^3 p}\left(\frac{3aev_t}{p} + 2\cos\theta\sqrt{\frac{\mu}{p}} - e\sqrt{\mu p}\sin\theta\right)^2\cdot\delta e \\
\dot{z}(\theta) &= \left(v_r\sin(\theta+\omega) + v_t\cos(\theta+\omega)\right)\cdot\delta i + \left(\sin i\left(-v_r\cos(\theta+\omega) + v_t\sin(\theta+\omega)\right)\right)\cdot\delta\Omega
\end{aligned}
\tag{4}
$$

given

$$\eta = \sqrt{1-e^2}$$

$p = a\left(1-e^2\right)$, semi-latus rectum

$r_c = \dfrac{p}{1+e\cos\theta}$, distance from the Sun to the asteroid at a given time, t

$v_r = \sqrt{\dfrac{\mu}{p}}e\sin\theta$, radial velocity of the spacecraft

$v_t = \sqrt{\dfrac{\mu}{p}}\left(1+e\cos\theta\right)$, tangential velocity of the spacecraft

where the orbital elements of the spacecraft are: a is the semi-major axis, e is the eccentricity, i is the inclination, Ω is the right ascension of the ascending node, ω is the argument of periapsis, θ is the true anomaly and M is the mean anomaly (as defined earlier), and μ is the gravitational constant of the Sun.

In order to minimize the required station-keeping of the spacecraft, a bounded, or periodic, orbit is advantageous. The bounded orbit is essentially one that will return to the same position after a fixed period of time and thus will not need any external control to maintain the spacecraft in the orbit. The conditions of periodicity are such that the period

of formation orbit must be equal to the period of the NEO in order not to incur any drift. This is done by setting the difference in semi-major axes equal to zero since the equation for the period of an orbit is a function of only the semi-major axis and gravitational constant, μ . By setting $\delta a = 0$, the variation of the mean anomaly δM becomes constant with time.

A periodic orbit can be found for almost any point in space surrounding the chief orbit. However, as in the case of any space mission, there are several mission-specific requirements that restrict the choice of the operational orbit, such as being in close proximity to the surface.

2.3. *Solar Sublimation Deflection Method*

One of the more interesting, and promising, methods for deviating asteroids is to use solar energy focused on a small spot on the asteroid surface which sublimates or melts the material thereby producing a thrust from the expelled matter. A number of previous studies have developed and compared the different deviation strategies (Sanchez Cuartielles *et al.*, 2007; Colombo *et al.*, 2006), including a preliminary analysis of the solar sublimation method using a mirror assembly onboard a formation of spacecraft (Maddock *et al.*, 2007). Due to symmetry, the deviation is the same whether the asteroid is accelerated or decelerated.

The mirror assembly developed is composed of three parts: a large parabolic reflector to focus the solar energy, a lens to collimate the beam, and a second flat pointing mirror to direct the beam onto the desired spot on the surface of the asteroid (see Fig. 3). In order to maximize the energy collected by the parabolic reflector, the reflector must always point directly at the Sun. As such, the required tilt angle of the secondary pointing mirror, relative to the normal axis of the parabolic mirror, is equivalent to the angle of reflection of the beam, α, shown in Fig. 3. This angle is constantly changing as the spacecraft orbits around the Sun.

Fig. 3. Configuration of the mirror assembly onboard a spacecraft to deviate an asteroid via solar sublimation, where α is the angle of reflection. The lens is placed just after the focal point of the parabolic mirror, depending on the desired beamwidth.

In a previous study, a trade-off was done between the size of the parabolic mirror, the number of spacecraft and the mission duration required to deviate different classes of asteroids by a fixed distance. Compared to the baseline approach of using a single spacecraft equipped with a very large parabolic mirror, it was found that using multiple spacecraft with smaller mirrors produced more potentially feasible results. One of the added complexities of using a spacecraft formation however is the coordination of the pointing mirrors to ensure the various spot beams overlap. While a margin of error is accounted for, the result of accumulative misalignment could mean that the energy density on the surface is not high enough to sublimate the material.

3. Optimal Formation Design Problem

The following section discusses the optimal formation design problem for the two test missions: a NEO tracking mission, and a NEO deviation mission. For both missions, the solution vector is defined as,

$$\xi = \begin{bmatrix} \delta e & \delta i & \delta\Omega & \delta\omega & \delta M \end{bmatrix}^T \tag{5}$$

with $\delta a = 0$ to guarantee the periodicity of the orbit.

3.1. *NEO Tracking Mission*

For a tracking mission, it is required that the spacecraft remains at an almost constant distance from the asteroid. At the same time it is desirable to see the asteroid from different angles. Therefore the problem is to design a periodic orbit that minimizes the difference between the minimum and the maximum distance from the center of the asteroid.

$$F_1 = \left\| \max\left(r_{cd}\right) - \min\left(r_{cd}\right) \right\| \tag{6}$$

Another desirable property of the formation would be to bring the plane of the orbit as close to the NEO as possible. This is implemented by minimizing the difference between the maximum distance at any point in the formation orbit, and a predetermined minimum distance r_{lim}.

$$F_2 = \left\| r_{lim} - \max\left(r_{cd}\right) \right\| \tag{7}$$

The radius of the limit sphere, r_{lim}, is the distance at which the gravity field of the asteroid is spherical and homogenous. Based on previous studies by Maddock *et al.* (2007) on the gravity model of Apophis, this limit is equal to 2.2983 km. At that distance, the gravity acceleration from the asteroid is about 2.5 E-7 m/s^2. In the following analysis, it was assumed that this disturbance would be compensated for by an active control system. The analysis and design of such a control system is beyond the scope of this paper and will be addressed in future work.

As the spacecraft cannot enter within the limit sphere of the asteroid however, an inequality constraint was imposed such that the minimum distance between the spacecraft and the NEO is always greater than the limiting radius,

$$C_{ineq} = r_{lim} - \min\left(r_{cd}\right) < 0 \tag{8}$$

Due to the dependant nature of the two objective functions, the optimization can be run as a single objective optimization. The overall objective function is simply a sum of the two equations for *F*,

$$\min_{\xi \in D} J_1 = \sum_{i}^{n} F_i = F_1 + F_2 \tag{9}$$

3.2. *NEO Deflection Mission*

The deflection mission uses two opposing objective functions based on the requirements of the flat pointing mirror in the spacecraft mirror assembly (see Fig. 3). The first is used to maximize the accuracy of the spot beam. The angular resolution required for the spot beam can be characterized by the following angle,

$$\sin\beta = \frac{d_{spot}}{2r_{cd}} = \frac{d_{mirror}\sin\alpha}{2r_{cd}} \tag{10}$$

which is a direct function of the distance of the satellite from the asteroid. Therefore, the first objective function J_1 for the deflection mission is the same as the one given in Equation (9).

The second requirement is to have a limited variation in the Sun-spacecraft-Asteroid angle α in order to minimize the effort of the attitude control system.

$$\alpha = 2\arccos\left(\frac{\langle \mathbf{r}_{cd}, \mathbf{r}_d \rangle}{r_{cd} r_d}\right) \tag{11}$$

Thus, the second objective function J_2 is defined as,

$$\min_{\xi \in D} J_2 = \max(\alpha) - \min(\alpha) \tag{12}$$

3.3. *Definition of the Search Space*

A number of boundary conditions were set to restrict the search space and improve the speed of the search. From inspection of the equations of motion, it is expected that the values of the $\delta\alpha$ parameters will be very close to 0. Due to the very small expected values, the inputs were scaled up closer to unity for the optimization process. Table 2 lists the upper and lower boundaries imposed on optimization of the solution vector.

Table 2. Boundaries on search space for the initial state vector ξ.

4. Optimization Procedure

The design of a formation made up of N satellites, all with optimal orbital characteristics, requires the identification not only of the global minimum but also of $(N-1)$ feasible local minima within a given search domain D. It is expected that for almost every position on the orbit, i.e. every instant of time, there are several optimal solution vectors that locally minimize the objective function. Therefore, a characterization of the search space for the problem in Equation (9) is required in order to find not only the global optimum but also a set of local optima with a value of the objective function close to the one of the global solution.

The second problem, instead, requires the identification of a set of feasible Pareto optimal solutions for the two objective functions in Equations (9) and (12). The two

problems share an important similarity: in both cases it is required to find a set of feasible solutions, rather than a single one, all with a particular property that defines their optimality.

To solve both problems, a hybrid behavioral-search approach was used that tries to collect into an archive A_g as many feasible solutions, either locally or Pareto optimal, as possible. The behavioral search is hybridized with a domain decomposition technique in order to extend the exploration of the search space.

In this section a general formulation for the two problems under study will be presented together with the main ideas implemented in the solution algorithm. A complete and detailed description of the proposed algorithm for the solution of unconstrained single objective problems can be found in Vasile and Locatelli (2007), Vasile (2007). In the following, an extension to multiobjective constrained algorithms will be presented.

4.1. *General Problem Formulation*

The general problem both for single and multiobjective optimization is to find a set X, contained in a given domain D, of solutions $\mathbf{u}$ such that the property $P(\mathbf{u})$ is true for all $\mathbf{u} \in X \subseteq D$,

$$X = \left\{ \mathbf{u} \in D \middle| P(\mathbf{u}) \right\} \tag{13}$$

where the domain D is a hyper-rectangle defined by the upper and lower bounds of the components of the vector $\mathbf{u}$,

$$D = \left\{ u_i \middle| u_i \in \left[b_i^l \quad b_i^u \right] \subseteq \mathbb{R}, i = 1,...,n \right\} \tag{14}$$

All the solutions satisfying property P are defined to be optimal with respect to P, or 'P-optimal', and X can be said to be a P-optimal set. Now, the property P might not identify a unique set, for example if P is the Pareto optimality then X can collect all the points belonging to a local Pareto front. Therefore we can define a global optimal set X_{opt} such that all the elements of X_{opt} dominate the elements of any other X,

$$X_{opt} = \left\{ \mathbf{u}^* \in D \middle| P(\mathbf{u}^*) \wedge \forall \mathbf{u} \in X \Rightarrow \mathbf{u}^* \prec \mathbf{u} \right\} \tag{15}$$

where $\mathbf{u}^* \prec \mathbf{u}$ represents the dominance of the $\mathbf{u}^*$ solution over the $\mathbf{u}$ solution.

If we are looking for local minima, the property P is to be a local minimizer, or a solution $\mathbf{u}^*$ can be said to dominate solution $\mathbf{u}$ if the associated value of the objective function $f(\mathbf{u}^*) < f(\mathbf{u})$. In this case X_{opt} would contain the global optimum or a set of global optima all with the same value of f. In the following we will look for the union of X and X_{opt}.

In the case of multiple objective problems, given a set of solution vectors we can associate to each one of them a scalar dominance index I_d such that,

$$I_d(\mathbf{u}_j) = \left| \left\{ i \middle| i \wedge j \in N_p \wedge \mathbf{u}_i \prec \mathbf{u}_j \right\} \right| \tag{16}$$

where the symbol |.| is used to denote the cardinality of a set and N_p is the set of the indices of all the given solution vectors. Here and in the following, a solution vector $\mathbf{u}_i$ is said to be dominating a solution vector $\mathbf{u}_j$ if the values of all the components of the objective vector $\mathbf{u}_i$ are lower than or equal to the values of all the components of the objective vector $\mathbf{u}_j$ and at least one component is strictly lower. In this case, for the j^{th} solution, $P(\mathbf{u}_j)$ simply defines the property of being not-dominated by any other solution in the set N_p, thus,

$$X = \left\{ \mathbf{u}_j \in D \middle| I_d(\mathbf{u}_j) = 0 \right\} \tag{17}$$

For constrained problems, the property P is to be optimal, either locally or Pareto, and feasible at the same time.

4.2. *Behavioral-Based Search*

A population of virtual agents is deployed in the search space. Each agent is associated to a solution vector **u** (in the particular case of the application presented in this paper, the solution vector is called ζ) and endowed with a set of basic actions forming a behavior. The entire population evolves through a number of steps toward the feasible set X. At each evolutionary step, the agents collect clues about the environment and implements actions according to an action selection mechanism. Some of these actions are devoted to acquiring new information, others to displacing agents toward the local minima, while other actions are instead used to exchange information among the agents.

The basic idea is that most of the bio-inspired global optimization approaches implement some form of basic behavior derived from nature: from mating of Evolutionary Algorithms (EA) to the flying of bird flocks in Particle Swarm Optimization (PSO) to the social behavior of ants in Ant Colony Optimization (ACO). Some of those behaviors can be classified as *social*, such as crossover in genetic algorithms, because they are devised to exchange pieces of information among the individuals. Other behaviors can be classified as *individualistic* because they aim at improving the individual status of each individual.

We implement a set of actions, each one producing an outcome $\mathbf{u}_{ke}$, derived from PSO, EA and DE (Differential Evolution) and a very simple, basic action selection mechanism (see Fig. 4). In particular, for individualistic behaviors, each agent can perform three types of actions: **A**, **B** and **C**. This general scheme accommodates two types of heuristics: Action **A** always generates the same outcome every time it is performed, once a solution vector **u** is given (e.g. inertia in PSO), while Actions **B** and **C** generate different values for the same **u** every time they are performed (e.g. mutation in EA). These last two actions are repeated until an improvement is registered or a maximum number of attempts is reached. The index k_e is increased by one every time an action is performed, and every action makes use of the agent status, the status of other agents and of the outcome of the preceding actions. For more details about the specific actions implemented here, the interested reader can refer to Vasile (2005a; 2005b; 2007), Vasile and Locatelli (2007).

Fig. 4. Action selection mechanism for individualistic behavior.

After an initialization is performed by sampling the solution space by Latin Hypercube, each solution vector is associated to an agent. Each agent is then evaluated and social behaviors (such as crossover) are implemented. After exchanging information with the other agents, each one can implement a set of individualistic actions (such as mutation, for example). The archive collects all the solutions for which *P* is true at every evolutionary step. Furthermore, at termination the entire population is added to the archive. Note that the property *P* required for feasible versus unfeasible agents is different: feasible agents are required to be either locally or Pareto optimal and to remain feasible, while unfeasible agents are required to simply become feasible. As a consequence, the entire population of agents is divided into two subpopulations: one aimed at being optimal, the other aimed at being feasible. The overall algorithm, called *Multiagent Collaborative Search* (MACS), is represented in Fig. 5 and briefly outlined in the following.

Multiagent Collaborative Search

Step 0. Initialization Generate an initial population of agents Π_0 within *D* through a Latin Hypercube (i.e., a non-collapsing design where points/agents are evenly spread even when projected along a single parameter axis; for a more detailed description and a justification of the use of Latin Hypercubes please refer, e.g., to van Dam *et al.* (2007)). A hyperrectangle $S^{\mathbf{u}_j^0}$ is associated to the j^{th} agent $\mathbf{u}_j^0 \in \Pi_0$. The initial *size* $\rho(\mathbf{u}_j^0)$ of each region $S^{\mathbf{u}_j^0}$ is fixed to 1 (i.e., the initial local region of each agent corresponds to the whole set *D*). The *effort* $s(\mathbf{u}_j^0)$ dedicated to agent $\mathbf{u}_j^0 \in \Pi_0$ is fixed to the same value s_{max} (equal to *n* in the computations) for all agents in Π_0. Set $k = 0$.

Step 1. Collaboration Agents collaborate with each other (social behavior). The collaborations give rise to a set of new solutions denoted by Q_{k+1}.

Step 2. Selection A subset of members of the set $\Pi_k \cup Q_{k+1}$ will be selected to give rise to the new updated population Π_{k+1}.

Step 3. Repulsion The population is updated through a repulsion mechanism: when the reciprocal distance of a number of agents goes below a given threshold, the worst one according to *P* is re-generated randomly within *D*.

Step 4. Filtering The population is ranked according to the assigned *P*. A *filter* partitions the population Π_{k+1} into two subsets: Π_{k+1}^{in}, the population fraction within the filter made of the best agents according to the property *P*, and Π_{k+1}^{out}, the population fraction outside the filter.

Step 5. Individualistic actions A set of actions, specified by a *behavior*, are applied to each agent $\mathbf{u}_j^{k+1} \in \Pi_{k+1}$. These allow local exploration (within $S^{\mathbf{u}_j^{k+1}}$) of the region around the agent. They are repeatedly applied until either an improvement is observed or the number of actions $s(\mathbf{u}_j^{k+1})$ exceeds the allowable threshold. If

an agent $\mathbf{u}_j^{k+1}$ generates an improvement, population Π_{k+1} is updated by replacing $\mathbf{u}_j^{k+1}$ with its improvement. The agents in Π_{k+1}^{in} versus Π_{k+1}^{out} perform different sequences of actions. In particular, the ones in Π_{k+1}^{out} only perform a random sampling of D through mutation.

Step 6. Hyperrectangle update The size parameter ρ and the effort parameter s associated to each agent within the filter are updated.

Step 7. Archive update Apply filtering and update archive A_l.

Step 8. Stopping rule A stopping rule is checked. If it is not satisfied, then set $k = k+1$ and go back to Step 1. If it is satisfied, then update the archive A_l by adding the current population, i.e., set $A_l = A_l \cup \Pi_{k+1}$.

Fig. 5. Overall algorithm for the Multiagent Collaborative Search (MACS).

The search is terminated after a given number of function evaluations. The overall algorithm combining the MACS and the domain decomposition technique is called *Evolutionary Programming and Interval Computation* (EPIC) (Vasile, 2005a; 2005b; 2007; Vasile and Locatelli, 2007). The code for EPIC, as well as all the models for the formation orbits, are implemented in Matlab® v.7.4.

4.3. *Domain Decomposition*

In the case of single objective optimization, the number of local minima is expected to be finite (for physical reasons). In the case of multiobjective optimization different portions of the Pareto front in the criteria space can correspond to different portions of the solution space. Therefore, the search space can be decomposed into a finite number of subsets, each containing a portion of the optimal set X such that $X \cap D \neq 0$. The initial domain D is progressively decomposed into smaller domains $D_l \subseteq D$ according to a decomposition strategy. The decomposition strategy is based on the output of the stochastic search step and produces a number M of subdomains D_l such that,

$$\bigcup_{l=1}^{M} D_l = D \tag{18}$$

Decomposition (18) is then iteratively applied to the subdomains D_l that need further exploration, so that

$$\bigcup_{l=1}^{M} D_l^{(d)} = D_l^{(d-1)} \tag{19}$$

where D is the decomposition depth.

Fig. 6. Hybrid domain decomposition and stochastic search.

In this implementation we use a simple regular cutting of each coordinate into two halves. Since the interest is to widely explore the search space and to collect as many elements of X as possible, after each stochastic search the largest subdomain D_l with the least number of collected samples belonging to X is selected for further decomposition, provided that the number of times its parent subdomains have already been decomposed without improvement (n_b) is below a given threshold.

We use the following merit function to balance the search of completely unexplored subdomains against those containing elements of X,

$$\Psi_{D_l} = (1-\upsilon)\varpi_{D_l} + \upsilon\phi_{D_l} \tag{20}$$

where ϖ_{D_l} is the density of already discovered solutions in D_l, ϕ_{D_l} is the best fitness in D_l, and υ is a weighting factor used to favor either convergence or exploration.

The partitioning cycle is stopped when a given number of subdomains have been generated, or when the maximum size of the archive has been exceeded. Note that in order to collect as many solutions belonging to X as possible while maintaining a low computational cost, we used a local archive A_l of limited size for each run of the MACS algorithm. We then store all the globally, non-dominated solutions for all the subdomains in a global archive, A_g.

4.4. *Single vs. Multiple Objective Optimization*

Although the problem formulation through the definition of P is general and applicable to both single objective (SOO) and multiple objective optimization (MOO) problems, either constrained or not, the actual property is substantially different depending on the type of problem.

For box constrained single objective problems, the property P is to be a local minimizer in D. If $S^{\mathbf{u}}$ is the local portion of the search space containing the agent $\mathbf{u}$, then the property can be formally expressed as follows,

$$f(\mathbf{u}) > f(\mathbf{u}_{k_e}) + \varepsilon \Rightarrow P(\mathbf{u}_{k_e}) = \text{true} \tag{21}$$

where ε is a minimum required local improvement.

For multiobjective problems, the property P is defined by the value of the scalar dominance index I_d,

$$I_d(\mathbf{u}) > I_{d,\varepsilon}(\mathbf{u}_{k_e}) \Rightarrow P(\mathbf{u}_{k_e}) = \text{true} \tag{22}$$

where ε is now the minimum expected improvement in the computation of the dominance. Note that this easily accommodates the concept of ε dominance.

Now, when multiple outcomes with the same dominance index are generated by either social or individualistic actions, the one that corresponds to the longest vector difference in the criteria space with respect to $\mathbf{u}$ is considered. Note that in many situations the action selection scheme in Fig. 5 generates a number of solutions that are dominated by the agent $\mathbf{u}$. Many of them can have the same dominance value; therefore in order to rank them, we use the modified dominance index,

$$I_d(\mathbf{u}_i) = \left|\left\{ j \,|\, f_j(\mathbf{u}_{k_e}) = f_j(\mathbf{u}) \right\}\right| \kappa + \left|\left\{ j \,|\, f_j(\mathbf{u}_{k_e}) > f_j(\mathbf{u}) \right\}\right| \tag{23}$$

where κ is equal to one if there is at least one component of $\mathbf{u}$ which is better than the corresponding component of $\mathbf{f}(\mathbf{u}_{k_e})$ and is equal to zero otherwise.

Now, if for the k_e^{th} outcome, the dominance index in Equation (23) is not zero but is lower than the number of components of the objective vector, then the agent $\mathbf{u}$ is only partially dominating the k_e^{th} outcome. Among all the partially dominated outcomes with the same dominance index, we chose the one that satisfies the condition,

$$\min_{k_e} \left\langle \left(\mathbf{f}(\mathbf{u}) - \mathbf{f}(\mathbf{u}_{k_e}), \hat{\mathbf{e}} \right) \right\rangle \tag{24}$$

where

$$\hat{\mathbf{e}} = \frac{\left[1, \quad 1, \quad ..., \quad 1\right]^T}{\sqrt{N_f}}$$

is the unit vector of dimension N_f, and N_f is the number of objective functions.

Since the partially dominated outcomes of one agent could dominate other agents or the outcomes of other agents at the end of every evolution cycle all the outcomes are added to the archive. Then, the dominance index in Equation (16) is computed for all the elements in A_l and only the non-dominated ones are preserved.

4.5. *Constraint Handling Technique*

The algorithm described above solves box-constrained problems. Since in most of the cases the imposed constraints are nonlinear, an extension of the algorithm was developed in order to account for nonlinear inequality constraints explicitly.

At each generation, the population of agents is divided into two subpopulations with a different P is assigned to each one, namely the property in Equations (21) or (22) is assigned to the subpopulation of feasible agents while the following property is assigned to the subpopulation of unfeasible agents:

$$F(\mathbf{u}) > F(\mathbf{u}_{k_e}) + \varepsilon \Rightarrow P(\mathbf{u}_{k_e}) = \text{true} \tag{25}$$

where

$$\min_{\mathbf{u} \in D} F = \sum_{j=1}^{m} \max\left(\left[0 \quad C_j \right] \right) \tag{26}$$

The two subpopulations are evolved in parallel and agents are allowed to migrate from one population to the other, i.e., if a feasible agent becomes unfeasible it is inserted in the subpopulation of unfeasible agents and assigned to the solution of the constraints. On the other hand, if an unfeasible agent becomes feasible it is inserted into the population of feasible agents and a different property P is assigned to it. As a result, the final optimal solution is either feasible or minimizes the infeasibility. This procedure does not maintain feasibility for any one of the agents. Feasibility can be preserved once

a feasible set has been found by defining the following augmented function F^* for the feasible agents:

$$\min_{\mathbf{u}\in D} F^* = \begin{cases} f & \text{if every } C_j \le 0 \\ f + \max(C) & \text{if any } C_j > 0 \end{cases} \tag{27}$$

The described strategy of co-evolving two populations with two different goals allows a flexible search for feasible optimal solutions; in fact through Equation (27) feasibility can be maintained on all or only part of the feasible solutions.

If all the feasible solutions are forced to remain feasible during the whole search process, the global exploration of the solution space may be penalized. The subpopulation of feasible agents could remain stuck in a niche along the boundary of the feasible region. Therefore, in order to search more extensively along the boundary of the feasible region, a subset of the feasible solutions is allowed to temporary violate the constraint and become unfeasible. Feasibility is always preserved only for the best agent.

Note that if in Equation (27), f is substituted with the dominance index I_d then the described constraint handling technique can be extended to the multiobjective case.

4.6. *Preliminary Optimization Test Cases*

The proposed optimization approach was extensively tested on several space-related problems with a single objective. For an experimental proof of effectiveness in the solution of single objective problems, the interested reader can refer to Vasile (2005a; 2007), Vasile and Locatelli (2007).

Here the interest is to apply EPIC at first to a single objective case and then to a multiobjective problem. Therefore a preliminary test was performed, applying EPIC to two well known multiobjective optimization problems in literature. For further details about these test functions, please refer to Deb *et al.* (2000; 2002).

Table 3. Parameters for the two preliminary test cases for EPIC.

The first test case, *DEB*, is a constrained multiobjective optimization problem with a convex Pareto front. The constraint C fragments the admissible Pareto front into a disconnected set. Running EPIC with a single level of branching and a limited population of 10 agents with 5 explorers, iterated for 12000 function evaluations, led to the result reported in Fig. 7 where the constraint is represented with a continuous line while the solutions found by EPIC are represented by points. The test was repeated 20 times with nearly identical results.

Fig. 7. Admissible Pareto front for the test case *DEB*. The constraint is represented by a continuous line, the points represent the solutions found by EPIC.

The second test case, *ZDT4*, is commonly recognized as one of the most challenging problems since it has 21^9 different local Pareto fronts of which only one corresponds to the global Pareto-optimal front. In this case the exploration capabilities of each single agents are enough to locate the correct front with very limited effort. In fact, even with just five agents it was possible to reconstruct the correct Pareto front 20 times over 20 different runs. The total number of function evaluations was fixed to 20000 for each of the runs (see Fig. 8b), although already after 10000 function evaluations EPIC was always able to locate the global front (see Fig. 8a).

Fig. 8. Admissible Pareto fronts for the test case *ZDT4*, (a) after 10000 function evaluations, (b) after 20000 function evaluations. The global Pareto-optimal front is represented by a continuous line, and the points represent the solutions found by EPIC.

Despite the small number of agents, the sampled points of the Pareto front are quite well distributed with just few, limited interruptions. The use of a limited number of agents instead of a large population is related to the complexity of the algorithm. In fact, the computational cost of the procedure for the management of the local archive A_l is of the order $n_A\left(n_p + n_A\right)$, where n_A is the archive size and n_p is the population size, while the cost of the implementation of the individualistic-social behaviors is of the order $n_p\left(n + n_p\right)$. Therefore, even if the overall algorithm is polynomial in the population dimension, the computational cost would increase quadratically with the number of agents. In the following tests, we used a local archive size of 600 which led to an average time for a single sweep of the EPIC algorithm of 0.1 s on an *Intel Centrino Due* 2.0 GHz with 1 Gb of RAM, the majority of which is required to handle the archive.

As an additional proof of the effectiveness of MACS, we compare the average Euclidean distance of 500 uniformly spaced points on the true optimal Pareto front from an equal number of points belonging to the solution found by EPIC with the analogous performance metric found in Deb *et al.* (2000) for NSGA-II, SPEA and PAES (see Table 4).

Table 4. Comparison of the average Euclidian distances between 500 uniformly space points on the optimal Pareto front for various optimization algorithms.

5. Experimental Results

5.1. *NEO Tracking Mission*

EPIC was initially run with a total of 20 agents exploring the search space. The number of subdomains was set to 14, with the weight υ equal to 0 to maximize exploration, and the maximum number of function evaluations per subdomain was set to 60000. Each function evaluation took 0.028 seconds on an *Intel Centrino Due* 2.0 GHz with 1 Gb of RAM. Although the result was quite good, achieving a value of the objective function of 2.93, we found that by re-optimizing locally with an SQP method we could further

improve the value of the best solution to 2.8997. The tolerance on the constraint was set equal to 10^{-6}, or 0.00000044%. Note that the aim is to design a set of optimal formation orbits. Therefore the algorithm is not required to run in real-time.

Fig. 9. Cross-comparison of the solution vector ξ for the SOO using EPIC.

Fig. 9 shows a cross-comparison between the different elements of the solution vector for 2182 possible solutions (or the total number of solutions generated from 10 independent runs). Note that we did not look for the minimum number of function evaluations for which EPIC was returning the best value with the desired accuracy. On the other hand, as will be shown in the following, the combination of domain decomposition and behavioral-based search was able to identify a number of very interesting families of solution. By comparison, running a local search with an SQP method from over 600 random samples and with a total number of function evaluations comparable to the one performed by EPIC, is not sufficient to identify all the families, although the best solution returned a value of 2.90.

Fig. 10. Range of all optimized values for the Objective Function J_1 from all runs.

Fig. 10 shows the variation in objective function J_1 across all the runs. It is clear that there are intervals where the value of the objective function is relatively constant. This is reflected by either only fractional changes in the orbital element differences in ξ, or is due to symmetry around the *y*-axis of the asteroid. Fig. 11 shows the values of the corresponding solution vector elements as the value of the objective function increases. The *solution index number* refers to the ranking of the solution vector ξ relative to increasing values of J_1 (the optimal value for J_1 has a solution index number of 1).

Fig. 11. Comparison of the values for the solution vector ξ for each of the results of the optimization.

Fig. 12 – Fig. 14 show the three families of optimal orbits. Within the same family, the difference in objective function is almost null while the differences in orbit geometry are significant. In particular, we can identify:

- four types of small symmetric orbits in Family A that are inclined with respect to the *x*-*y* plane (see Fig. 12),
- two types of symmetric orbits in Family B that have a small inclination with respect to the *x*-*y* plane (see Fig. 13),
- two types of large symmetric orbits in Family C that are inclined with respect to the *x*-*y* plane and encircle the asteroid (see Fig. 14).

Fig. 12. Orbital geometry of solutions from Family A, $J_1 \approx 2.9$.

Fig. 13. Orbital geometry of solutions from Family B, $J_1 \approx 45.6$.

Fig. 14. Orbital geometry of solutions from Family C, $J_1 \approx 80.4$.

The orbital diagrams are all shown in the rotating relative Hill reference frame, where the radial axis $\hat{x}$ is the direction from the Sun to the asteroid, the normal axis $\hat{z}$ is the direction of the angular momentum of the spacecraft, and the transversal axis $\hat{y}$ is completing the triad. In the three orthographic views, the top figure (a) of the *x*-*y* plane shows the view looking 'down' on the ecliptic plane. The second plot (b) in the *x*-*z* plane is from the point-of-view of the asteroid looking out at the formation, and the lastly the *y*-*z* plot (c) is the view looking out from the Sun. For each of the diagrams, the asteroid is located at the center point $(0,0)$ and the small circle on each orbit represents the position of the spacecraft at a specific point in time. The corresponding values of the objective function and solution vectors in Fig. 12 – Fig. 14 are given in Table 5.

As can be seen, the spatial separation among the spacecraft in the second family of orbits is tiny. Such a small separation does not allow for an improvement in the tracking measurements due to multiple tracking signals. On the other hand, the first family of orbits can easily accommodate four different spacecraft. In addition, by exploiting the symmetry of the Family B, another two satellites can be added, with a further four more from the third family. The first two families of formation orbits are also quite interesting for the NEO deflection application.

Table 5. Values for the best results for each family of objection function J_1 and the corresponding solution vector ξ.

5.2. *NEO Deflection Mission*

Through the optimization of the single objective function, we identified three families of formation orbits with different characteristics and values of the objective function J_1. Families A and B are very close to the asteroid and are particularly interesting for a deflection mission because they provide a particularly advantageous position from which the sunlight can be focused onto the surface of the asteroid. Moreover, the Sun-spacecraft-Asteroid angle is nearly the same for all the spacecraft, which allows them all to have a similar attitude control. Starting from the solutions of the first family, we computed the whole set of Pareto optimal solutions that simultaneously attempt to minimize J_1 and J_2. EPIC was run for 40000 function evaluations with 20 agents and no domain decomposition. Each function evaluation took 0.035 seconds on an intel Centrino Due 2.0Ghz with 1Gb of RAM

Fig. 15. Cross comparison of the solution vector ξ for the MOO using EPIC.

Fig. 15 shows a cross-comparison between the different elements of the solution vector for the whole Pareto set. Fig. 16 shows the Optimal Pareto front for the multiobjective optimization. The best group of solutions of the single objective case would be in the upper left part of the Pareto front, all with very similar values for the objective function J_2.

Fig. 16. Optimal Pareto front for MOO illustrating the trade-off in accuracy of the beam. The red circles represent the two solution points given in Table 5.

Fig. 17 shows the orbit with the first objective function J_1 minimized. This represents the formation orbit closest to the asteroid, with the minimum difference between the closest and farthest points from the asteroid. By comparison, Fig. 18 shows the orbit minimizing the second objective function, J_2. The spacecraft is moving back and forth along an orbit which is stretched in the direction of the y-axis and, as such, only requires minute adjustments in the directional mirror.

Table 6. Values for the objective functions and solution vector ξ for the end limits of the Pareto front for the MOO.

Table 6 shows the corresponding values for the objective functions and state vector. Note that for the latter solution, although the difference between the farthest point and the closest point is higher then for the former solution, the whole trajectory on average, is still quite close to the asteroid.

Fig. 17. Formation orbit minimizing the J_1 value.

Fig. 18. Formation orbit minimizing the J_2 value.

6. Conclusion

This paper presents the design for determining optimal orbits for one or multiple spacecraft flying in formation with an asteroid. Two cases were presented: an asteroid tracking mission and a NEO deflection mission. For the former mission, three families of optimized symmetric orbits were found, all in close proximity to the asteroid with minimal variation in distance in order to minimize the pointing errors of the measurement devices. The different characteristics of the three families allows for the design of a constellation of tracking satellites with a consequent improvement of the tracking signal due to multiple measurements. Relaxing the requirement on the minimum distance from the asteroid would allow for the design of different variants within each family.

The three families of solutions found for the tracking mission represent a portion of the set of Pareto optimal solutions for the second case, the NEO deflection mission. All the orbits have a maximum variation of the pointing angle of 5°, which requires only a very limited effort from the attitude control system. The distribution of the $\delta\alpha$ parameters for these orbits suggests that with small variations of $\delta\Omega$ and $\delta\omega$, the separation can be tuned without any major variation in either objective function.

The analysis presented in this paper was limited to one single asteroid with particular orbit characteristics. A more extensive analysis considering a wide range of asteroids is ongoing and the results will be present in future papers.

References

Bottke, Jr., W. and Vokrouhlický, D., Rubincam, D., Brož, M. (2002). The Effect of Yarkovsky Thermal Forces on the Dynamical Evolution of Asteroids and Meteoroids, *Asteorids* **III**: 395–408

Chesley, S. R. (2005). Potential impact detection for Near-Earth asteroids: The case of 99942 Apophis (2004 MN4), *Asteroids, Comets, Meteors Proceedings*, IAU Symposium **229**: 215–228.

Coello, C. A. C. and Lamont, G., Van Veldhuizen, D. (2007). *Evolutionary Algorithms for Solving Multi-Objective Problems*, 2nd Edition, Springer, New York.

Colombo C. and Sanchez Cuartielles J. P. , Vasile M. , Radice G. (2006). A Comparative Assessment of Different Deviation Strategies for Dangerous NEOs, *56th International Astronautical Congress*, Valencia, Spain, IAC-06-A3.P.05.

Council of Europe (1996). Resolution 1080: Recommendations on the detection of asteroids and comets potentially dangerous to humankind.

Deb, K. and Pratap, A., Meyarivan, T. (2000). Fast elitist multi-objective genetic algorithm: NGA-II, KanGAL Report No. 200001.

Deb, K. and Pratap, A., Meyarivan, T. (2002). Constrained test problems for multi-objective evolutionary optimization, KanGAL Report No. 200002.

Elbeltagi, E. and Hegazy, T., Grierson, D. (2005). Comparison among five evolutionary-based optimization algorithms, *Advanced Engineering Informatics* **19**: 43–53.

Global Science Forum (2003). *Final Report from the Workshop on NEOs: Risks, Policies and Actions*, Organization for Economic Co-operation and Development.

Kennedy J. and Eberhart, R. (1995). Particle swarm optimization, *Proceedings of the IEEE International Conference on Neural Networks*: 1942–1948.

Maddock, C. and Sanchez Cuartielles, J.P., Vasile, M., Radice G. (2007). Comparison of Single and Multi-Spacecraft Configurations for NEA Deflection by Solar Sublimation, *New Trends in Astrodynamics and Applications III*, American Institute of Physics Conference Proceedings **886**: 303–316.

Melosh, H. J. and Nemchinov, I. V., Zetzer, Y. (1994). Non-nuclear Strategies for Deflecting Comets and Asteroids, *Hazard Due to Comets and Asteroids*: 1110–1131.

NASA Near Earth Object Program (2008). *99942 Apophis (2004 MN4) Impact Risk* (online resource), http://neo.jpl.nasa.gov/risk/a99942.html, link valid as of 01 January 2008.

Near-Earth Object Mission Advisory Panel (2004). *Space Mission Priorities for Near-Earth Object Risk Assessment and Reduction*, European Space Agency (ESA) Report.

Price K. V. and Storn, R. M., Lampinen, J. A. (2005). Differential Evolution: A Practical Approach to Global Optimization, Springer.

Sanchez Cuartielles J. P. and Colombo C., Vasile M., Radice G. (2007). A Multi-criteria Assessment of Deflection Methods for Dangerous NEOs, *New Trends in Astrodynamics and Applications III*, American Institute of Physics Conference Proceedings **886**: 317–333.

Schaub, H. and Junkins, J. L. (2003). *Analytical Mechanics of Space Systems*, AIAA Education Series, Virginia, USA.
Schweickart, R. L. (2005). *A Call to (Considered) Action*, International Space Development Conference, B612 Foundation Occasional Paper 0501.
Sierra, M. R. and Coello, C. A. C. (2007). A Study of Techniques to Improve the Efficiency of a Multi-Objective Particle Swarm Optimizer, *Evolutionary Computation in Dynamic and Uncertain Environments*: 269–296.
Vallado, D. A. (2007). *Fundamentals of Astrodynamics and Applications*, 3rd Edition, Space Technology Library, Microcosm Press, California, USA and Kluwer Academic Publishers, The Netherlands.
van Dam, E. R. and Husslage, B., den Hertog, D., Melissen H. (2007). Maximin Latin Hypercube Designs in Two Dimensions, *Operations Research* **55**: 158–169.
Vasile, M. (2005a). A Hybrid Multi-Agent Collaborative Search Applied to the Solution of Space Mission Design Problems, *Global Optimization Workshop*.
Vasile, M. (2005b). Robust Mission Design Through Evidence Theory and Multiagent Collaborative Search, *Annals of the New York Academy of Sciences* **1065**: 152–173.
Vasile, M. (2007). A Behavioral-based Meta-heuristic for Robust Global Trajectory Optimization, *IEEE Congress on Evolutionary Computing (CEC-07) Proceedings*: 2056–2063.
Vasile, M. and Locatelli, M. (2007). A hybrid multiagent approach for global trajectory optimization, *Journal of Global Optimization*, accepted, to appear.

About the authors

Dr. Massimiliano Vasile is the corresponding author and can be contacted at m.vasile@aero.gla.ac.uk.

DR. MASSIMILIANO VASILE received his Master and Ph.D. degrees from the Department of Aerospace Engineering of Politecnico di Milano, Italy, in 1996 and 2000 respectively. From 2001 to 2003 he worked as Research Fellow in the Advanced Concepts Team of the European Space Agency (ESA), on new methods for Space Mission Analysis and Design and Trajectory Optimization. From 2004 to 2005 he worked as a lecturer in Space System Engineering in the Department of Aerospace Engineering of Politecnico di Milano. Since 2005, he has been a Lecturer in the Department of Aerospace Engineering and Head of Research for the Space Advanced Research Team at the University of Glasgow (http://www.aero.gla.ac.uk/Research/SpaceArt). His main research interests are: Space Mission Analysis and Design, Global and Multiobjective Optimization, Bio-inspired Optimization Methods, Asteroids, Evolutionary Computation, Concurrent Engineering, Multidisciplinary Design, Swarm Intelligence, Formation Flying, Autonomous Robotic Systems. He is member of the IEEE, AIAA and AIRO. Email: m.vasile@aero.gla.ac.uk

MS. CHRISTIE MADDOCK received her B.Eng. Honours degree in Aerospace Electronics and Systems Engineering from Carleton University, Canada in 2002, and is currently working towards her doctorate degree with the Space Advanced Research Team at the University of Glasgow in the UK. Her research interests are Dynamics and Control, Spacecraft Formation Flying, Evolutionary Computing and Game Theory, Space-based Communication Systems and Space Mission Analysis and Design. She is a member of the IEEE and BIS.

Table 1. Estimated and observed orbital and physical properties Apophis 99942

Element	Measurement value	Uncertainty, 1σ
Semi-major axis, *a*	0.9223 AU	2.4336 E-8
Eccentricity, *e*	0.1911	7.5675 E-8
Inclination, *i*	3.3313 deg	2.0247 E-6
Period, *T*	323.50 days	1.2805 E-5
Mean motion, *n*	1.1128 deg/day	4.4047 E-8
Ellipsoidal dimensions	226 m × 160 m × 113 m	0.06

[a] The physical dimensions are calculated assuming an ellipsoidal model for the asteroid, based on the observed magnitude.
[b] The uncertainty is calculated for one standard deviation.

Table 2. Boundaries on search space for the initial state vector, ξ

Element in Initial State Vector		Lower Bound	Upper Bound
Difference in Eccentricity (10^{-7})	δe	-0.1	0.1
Difference in Inclination (10^{-7} rad)	δi	-0.1	0.1
Difference in Right Ascension of the Ascending Node (10^{-7} rad)	$\delta\Omega$	$-\pi$	π
Difference in Argument of Periapsis (10^{-7} rad)	$\delta\omega$	$-\pi$	π
Difference in Mean Anomaly (10^{-7} rad)	δM	$-\pi$	π

Table 3. Parameters for the two preliminary test cases for EPIC.

ID	Parameters	Objective Function and Constraints
DEB	$y \in [0 \quad 1]$ $i = 1,...,n$ $a = 0.2 \quad b = 10$ $c = 1 \quad d = 6$ $e = 1 \quad n = 10$	$f_1 = y_1$ $f_2 = g\left(1 - \sqrt{\frac{f_1}{g}}\right) + 1 \quad \text{given} \quad g = 1 + \frac{9}{n-1}\sum_{i=2}^{n} y_i$ $C = (f_2 - e)\cos\theta - f_1 \sin\theta - a\left\lvert \sin\left(b\pi\left((f_2 - e)\sin\theta - f_1\cos\theta\right)^c\right)\right\rvert^d$
ZDT4	$y \in [0 \quad 1]$ $y_i \in [-5 \quad 5]$ $i = 2,...,n$ $n = 10$	$f_1 = y_1$ $f_2 = g\left(1 - \sqrt{\frac{f_1}{g}}\right) \quad \text{given} \quad g = 1 + 10(n-1) + \sum_{i=2}^{n}\left(y_i^2 - 10\cos(4\pi y_i)\right)$

Table 4. Comparison of the average Euclidian distances between 500 uniformly space points on the optimal Pareto front for various optimization algorithms

Approach	Average Euclidian Distance	Standard Deviation
EPIC	1.542 E-3	5.19 E-4
NSGA-III	0.513053	0.118460
SPEA	7.340299	6.572516
PAES	0.854816	0.527238

Table 5. Values for the best results for each family of objective function J_1 and the corresponding solution vector ξ.

Objective Function		$J_1 = 2.8997$	$J_1 = 45.5922$	$J_1 = 80.4110$
Difference in Eccentricity	$\xi(1) = \delta e$	1.3629 E-9	7.2294 E-8	4.0447 E-7
Difference in Inclination (rad)	$\xi(2) = \delta i$	0.01671	0.0006949	-0.08853
Difference in Right Ascension of the Ascending Node (rad)	$\xi(3) = \delta\Omega$	-0.3908	-0.005114	2.0699
Difference in Argument of Periapsis (rad)	$\xi(4) = \delta\omega$	0.3070	-0.07934	-1.6261
Difference in Mean Anomaly (rad)	$\xi(5) = \delta M$	-0.08197	-0.08289	-0.4342

Table 6. Values for the objective functions and solution vector ξ for the end limits of the Pareto front for the MOO.

Element		Value with optimal J_1	Value with optimal J_2
Objective Function for r_{cd}	J_1	2.8997	1558.01
Objective Function for α	J_2	0.095905	2.7719 E-5
Difference in Eccentricity	$\xi(1)=\delta e$	1.3629 E-9	4.5655 E-6
Difference in Inclination (rad)	$\xi(2)=\delta i$	0.01671	-0.03557
Difference in Right Ascension of the Ascending Node (rad)	$\xi(3)=\delta\Omega$	-0.3908	0.09568
Difference in Argument of Periapsis (rad)	$\xi(4)=\delta\omega$	0.3070	-0.3011
Difference in Mean Anomaly (rad)	$\xi(5)=\delta M$	-0.08197	-1.5409 E-5

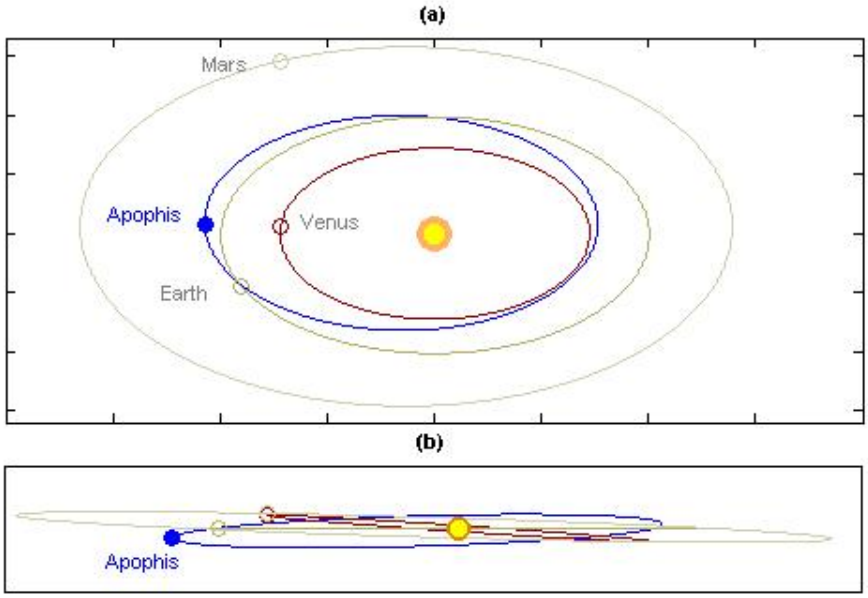

Fig. 1. Orbit of the NEO Apophis, compared to the orbits of Mars, Earth and Venus. The top figure (a) illustrates the view of the ecliptic plane, the bottom figure (b) shows the inclination difference between the orbits.

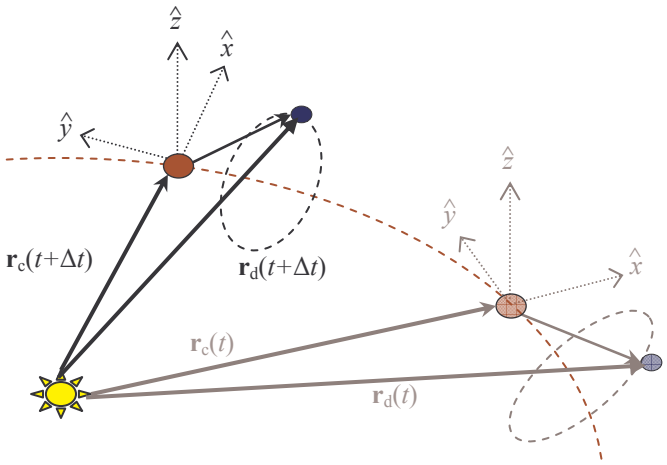

Fig. 2. Illustration of a chief orbit and a relative deputy spacecraft orbit flying in formation at two instants in time, t and $(t+\Delta t)$. The vector from the Sun to the asteroid (or chief) in inertial coordinates is given by $\mathbf{r}_c$, and from the Sun to the formation, or deputy, spacecraft by $\mathbf{r}_d$

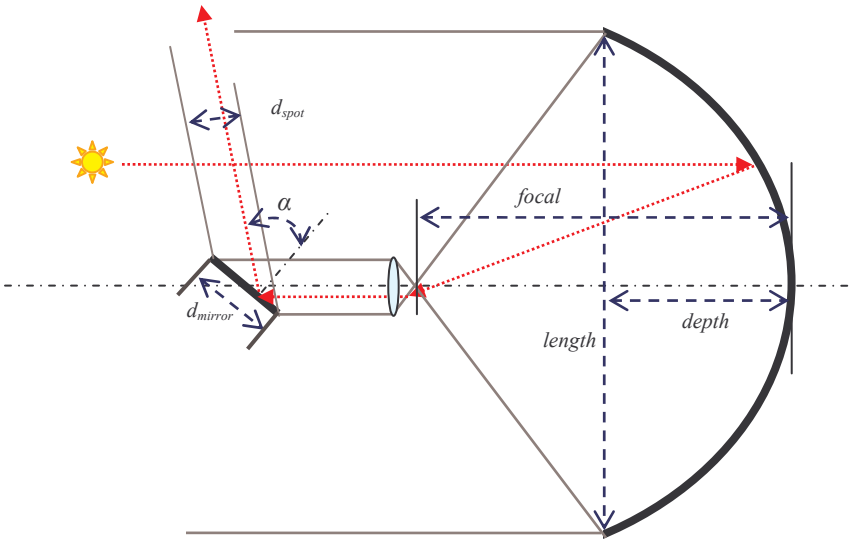

Fig. 3. Configuration of the mirror assembly onboard a spacecraft to deviate an asteroid via solar sublimation, where α is the angle of reflection. The lens is placed just after the focal point of the parabolic mirror, depending on the desired beamwidth

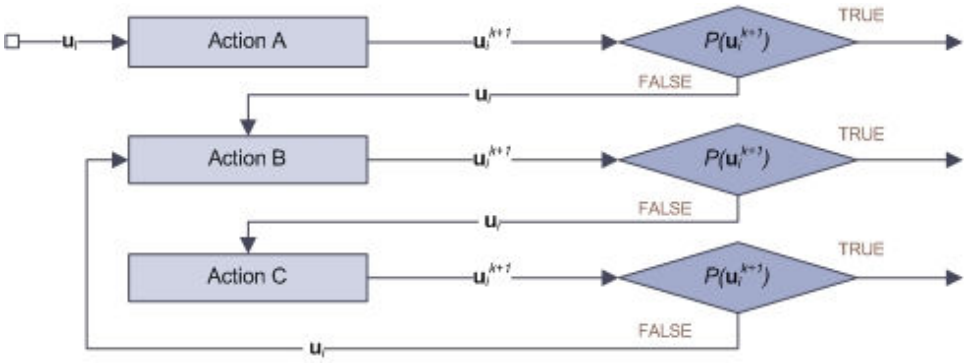

Fig. 4. Action selection mechanism for individualistic behavior

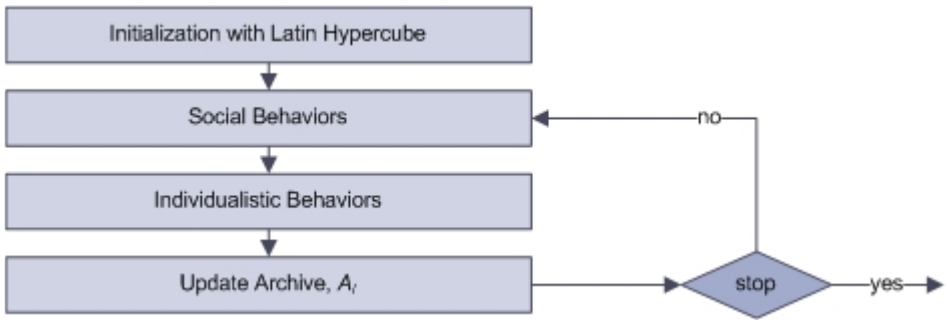

Fig. 5. Overall algorithm for the Multiagent Collaborative Search (MACS).

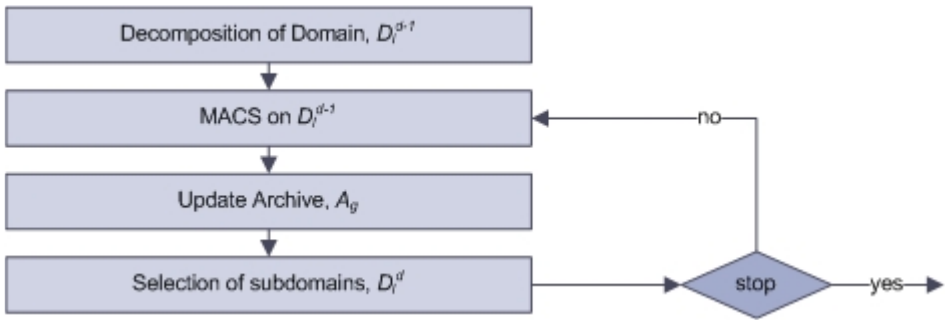

Fig. 6. Hybrid domain decomposition and stochastic search.

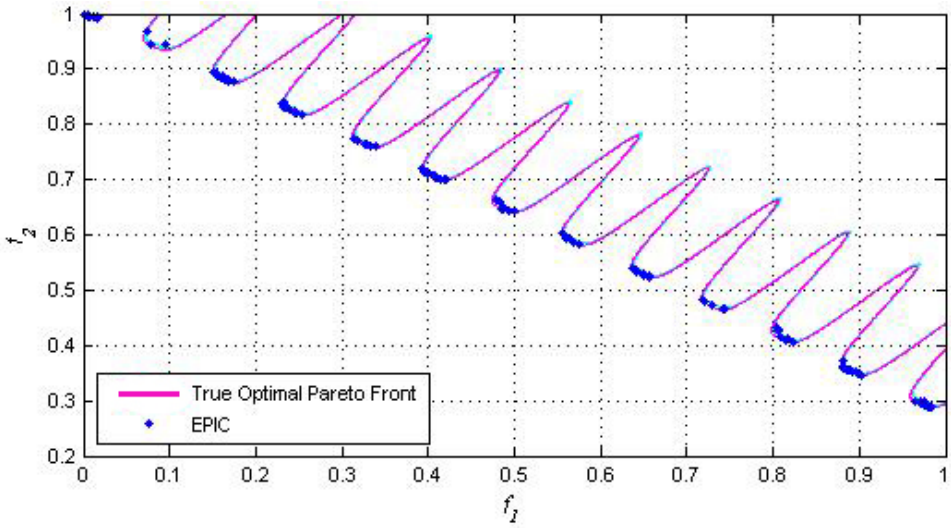

Fig. 7. Admissible Pareto front for the test case *DEB*. The constraint is represented by a continuous line, the points represent the solutions found by EPIC.

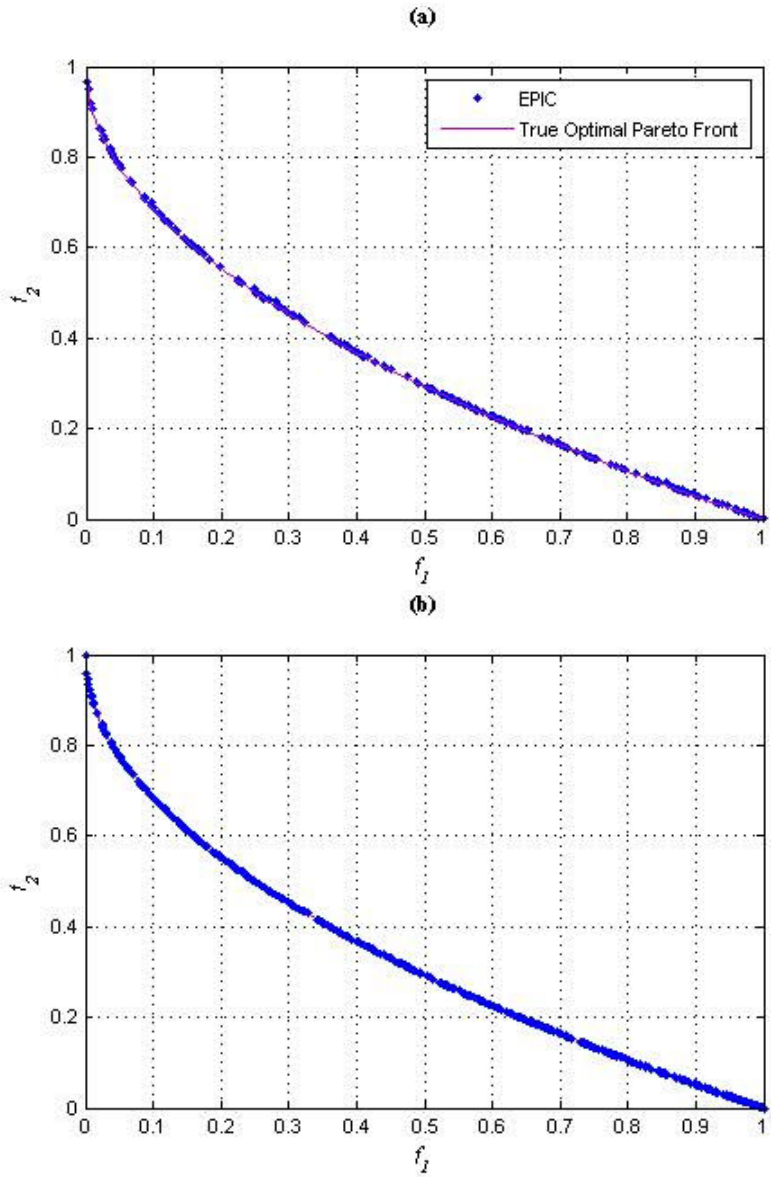

Fig.8. Admissible Pareto fronts for the test case *ZDT4*, (a) after 10000 function evaluations, (b) after 20000 function evaluations. The global Pareto-optimal front is represented by a continuous line, and the points represent the solutions found by EPIC.

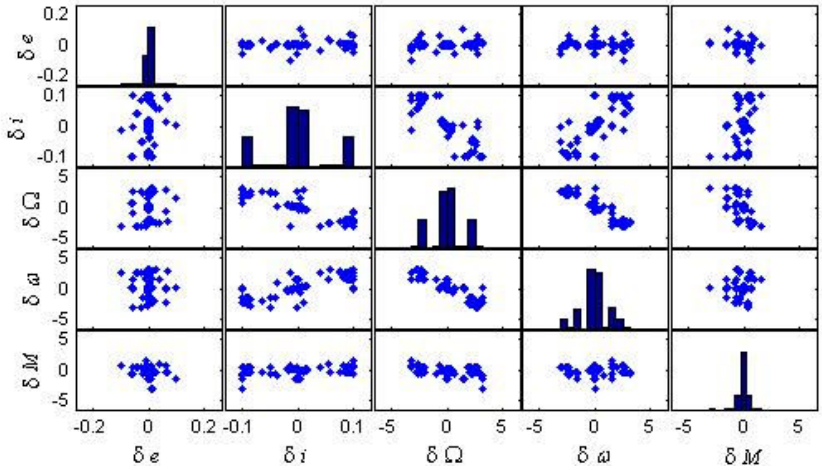

Fig. 9. Cross-comparison of the solution vector ξ for the SOO using EPIC.

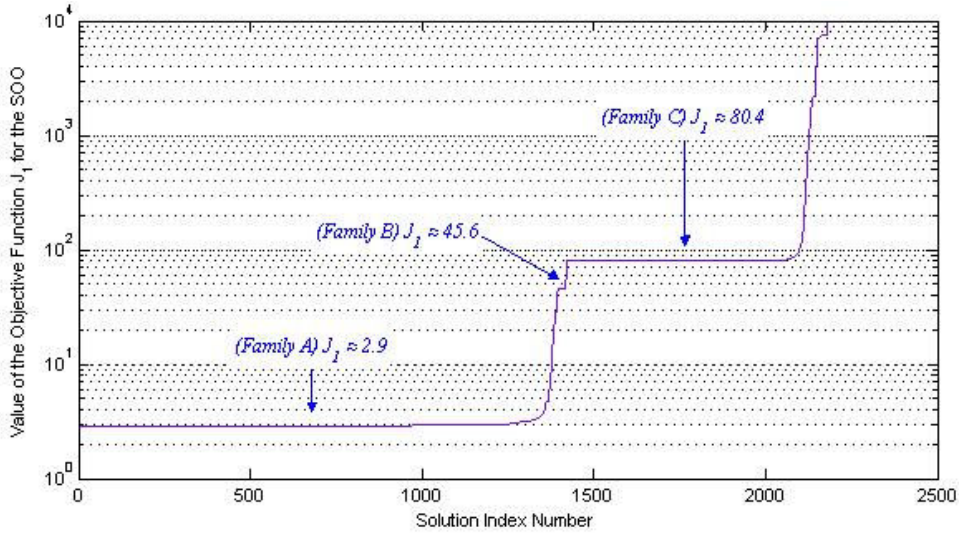

Fig.10. Range of all optimized values for the Objective Function J_1 from all runs.

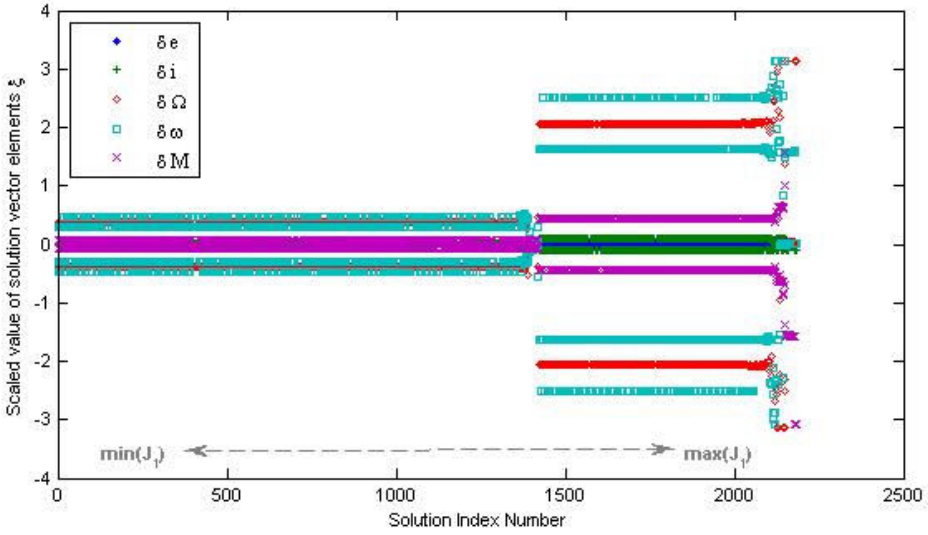

Fig.11. Comparison of the values for the solution vector ξ for each of the results of the optimization.

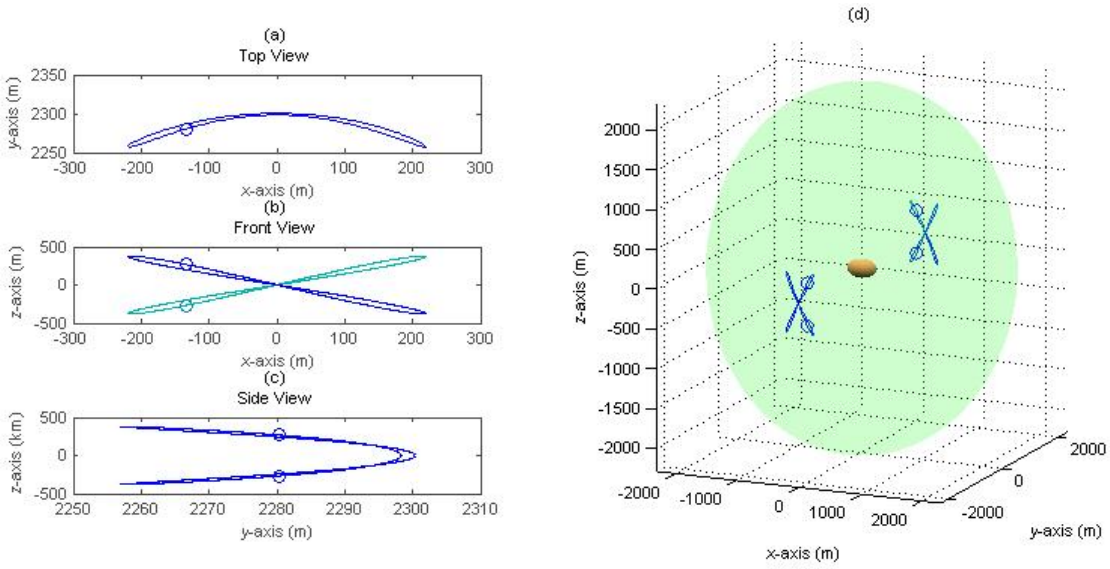

Fig.12. Orbital geometry of solutions from Family A, $J_1 \approx 2.9$.

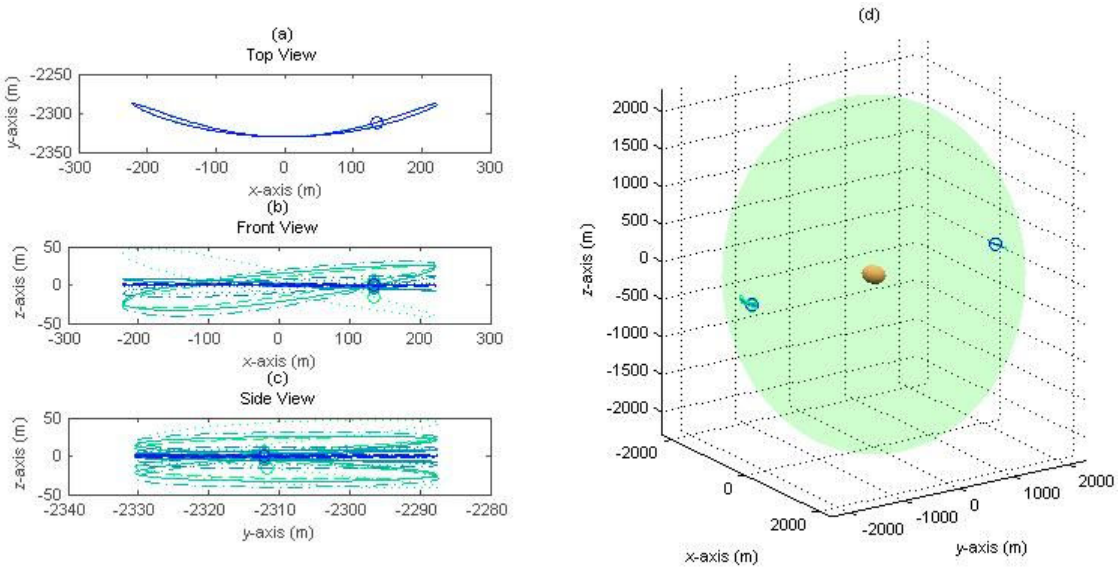

Fig.13. Orbital geometry of solutions from Family B, $J_1 \approx 45.6$.

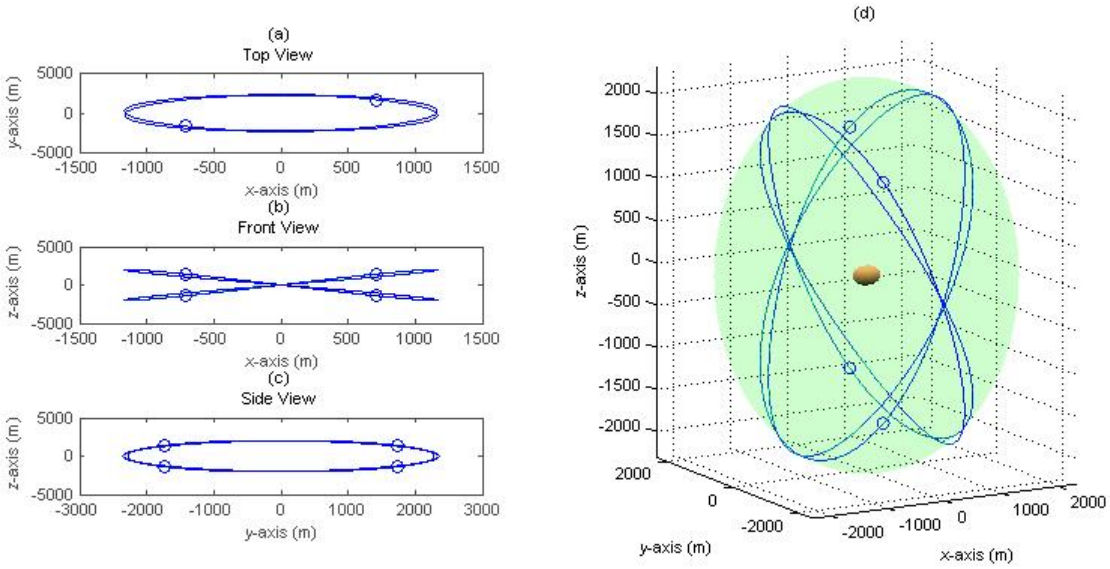

Fig.14. Orbital geometry of solutions from Family C, $J_1 \approx 80.4$.

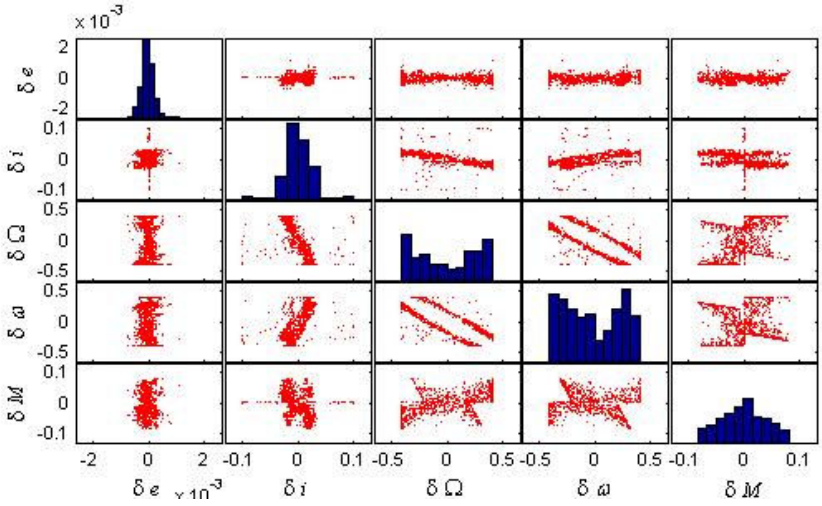

Fig.15. Cross comparison of the solution vector ξ for the MOO using EPIC.

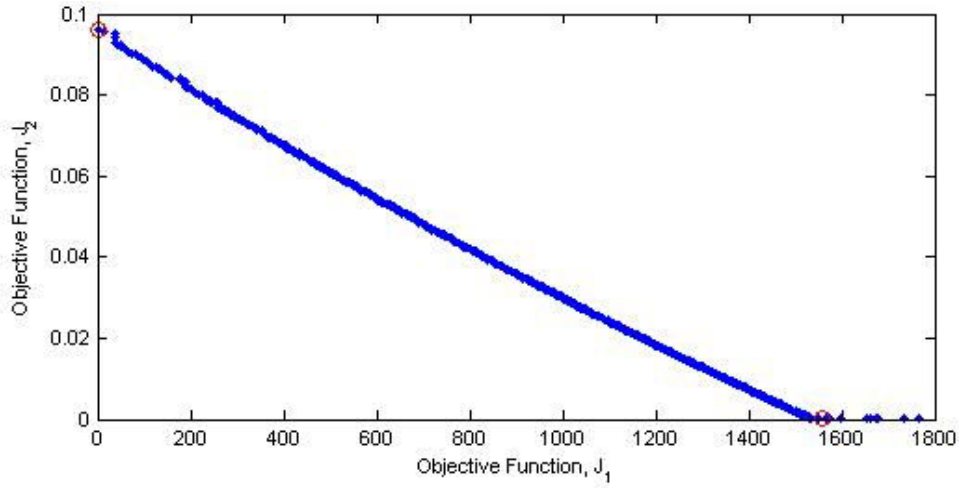

Fig.16. Optimal Pareto front for MOO illustrating the trade-off in accuracy of the beam. The red circles represent the two solution points given in Table 5.

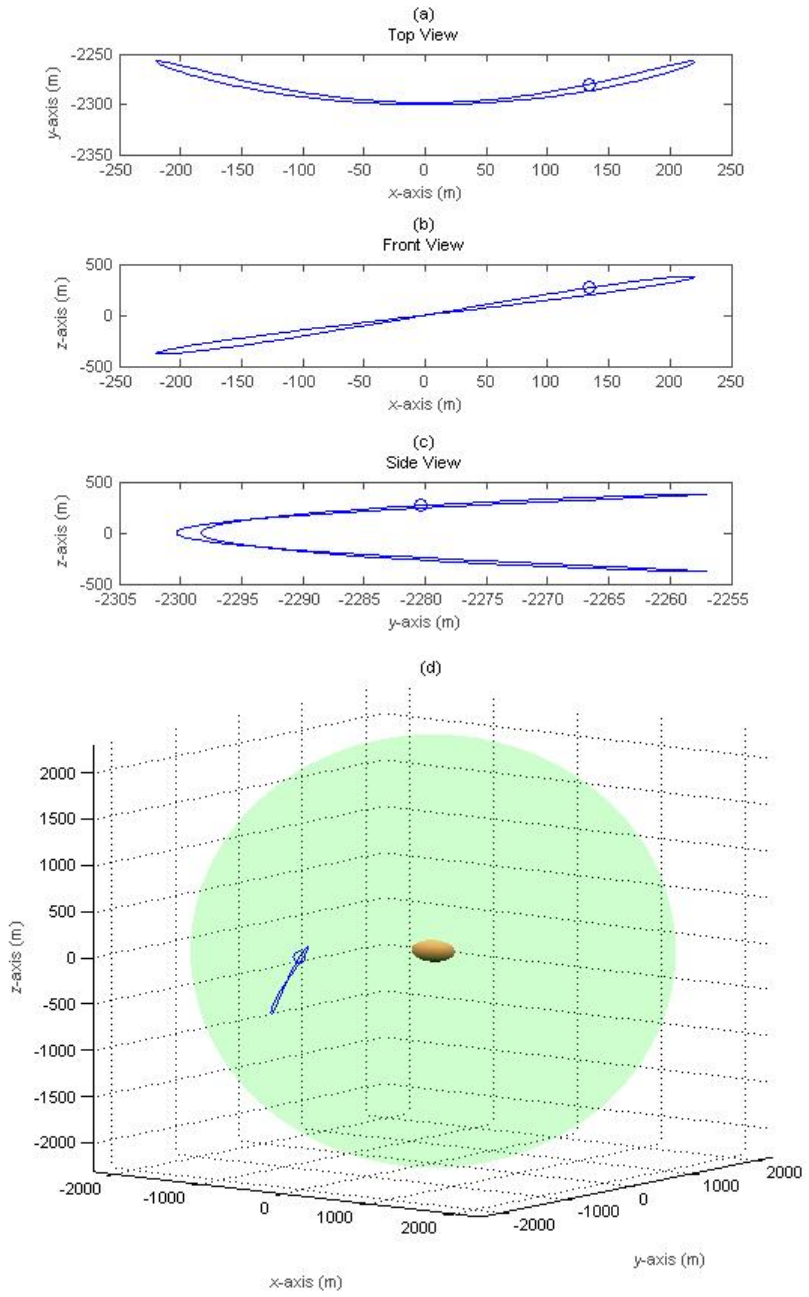

Fig.17. Formation orbit minimizing the J_1 value.

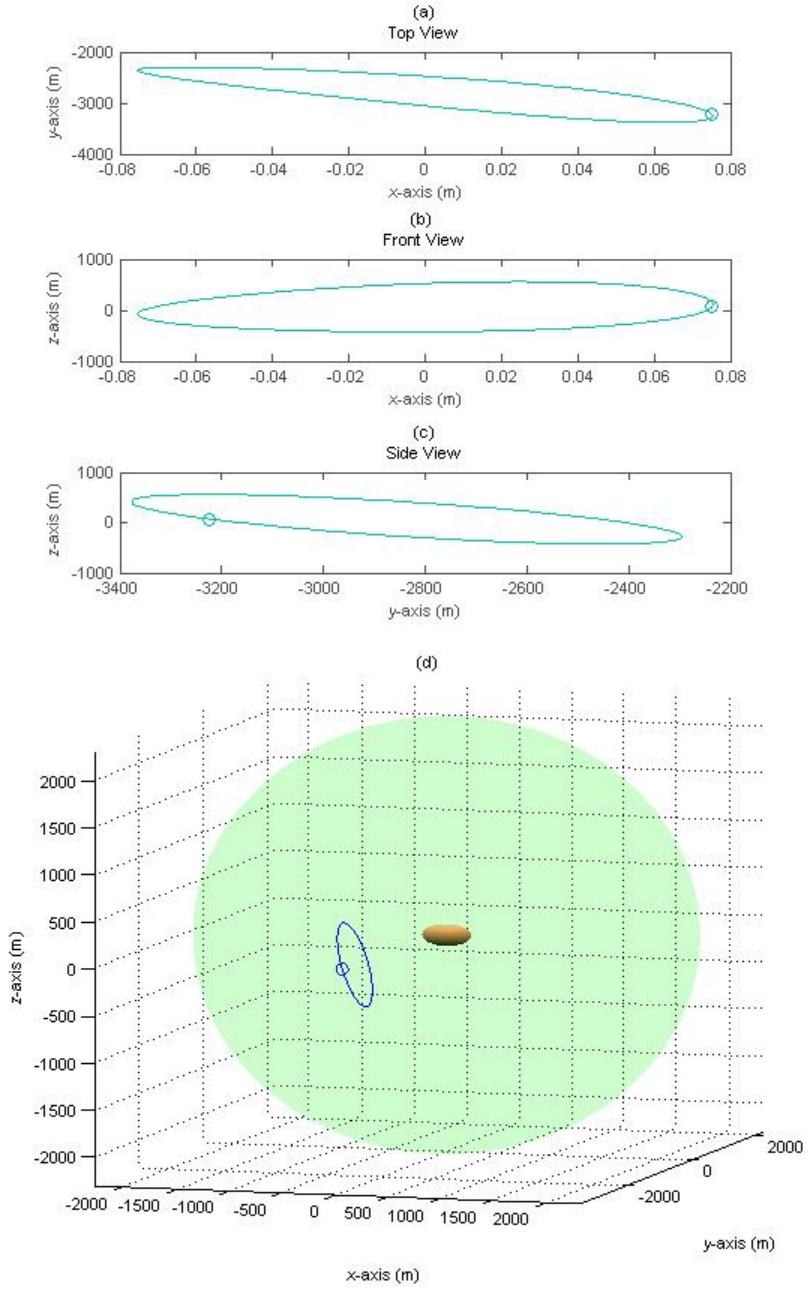

Fig.18. Formation orbit minimizing the J_2 value.